Dynamics in colloidal liquids near a crossing of glass- and gel-transition lines

M. Sperl
Physik Department, Technische Universität München, 85747 Garching, Germany
(Received 19 August 2003; published 15 January 2004)

Within the mode-coupling theory for ideal glass transitions, the mean-squared displacement and the correlation function for density fluctuations are evaluated for a colloidal liquid of particles interacting with a square-well potential for states near the crossing of the line for transitions to a gel with the line for transitions to a glass. It is demonstrated how the dynamics is ruled by the interplay of the mechanisms of arrest due to hard-core repulsion and due to attraction-induced bond formation as well as by a nearby higher-order glass-transition singularity. Application of the universal relaxation laws for the slow dynamics near glass-transition singularities explains the qualitative features of the calculated time dependence of the mean-squared displacement, which are in accord with the findings obtained in molecular-dynamics simulation studies by Zaccarelli *et al.* [Phys. Rev. E **66**, 041402 (2002)]. Correlation functions found by photon-correlation spectroscopy in a micellar system by Mallamace *et al.* [Phys. Rev. Lett. **84**, 5431 (2000)] can be interpreted qualitatively as a crossover from gel to glass dynamics.

DOI: 10.1103/PhysRevE.69.011401 PACS number(s): 82.70.Dd, 61.20.Lc, 64.70.Pf

I. INTRODUCTION

The mode-coupling theory for ideal glass transitions (MCT) is based on closed equations of motion for the correlation functions of the density fluctuations $\rho_{\vec{q}}$ of wave vector $\vec{q}$, $\phi_q(t)=\langle\rho_{\vec{q}}^*(t)\rho_{\vec{q}}\rangle/\langle|\rho_{\vec{q}}|\rangle$, $q=|\vec{q}|$ [1,2]. The static structure factor S_q enters these equations as input; it is assumed to be a smooth function of the control parameters like density ρ or temperature T. The equations of motion exhibit bifurcations for the long-time limit of the correlators, $f_q=\lim_{t\to\infty}\phi_q(t)$, which are referred to as glass-transition singularities. Only bifurcations of the cuspoid family can occur in the MCT equations [2,3], i.e., singularities of the class A_l, $l\geqslant 2$, which are equivalent to the bifurcations in the real roots of real polynomials of order l [4]. The generic singularity when changing a single control parameter is the A_2, also called fold. In the most important situations, it deals with the transition from a liquid, characterized by $f_q=0$, to an idealized glass, characterized by $f_q>0$. The quantity f_q is the Debye-Waller factor for the arrested amorphous structure. For parameters near a glass-transition singularity, slow dynamics emerges with subtle dependence on time and control parameters. This dynamics is proposed by MCT as the explanation for the structural relaxation in glass-forming liquids. The universal laws for this dynamics can be obtained by asymptotic expansion of the equations of motion as was demonstrated comprehensively for the hard-sphere system (HSS) [5,6]. The glass transition for the HSS has been studied experimentally by dynamic light scattering for sterically stabilized hard-sphere colloids [7–9]. The successful analysis of the data within the MCT frame provides strong support for the theory [10].

It is known from studies of so-called schematic models that there may emerge also higher-order singularities from MCT such as A_3 and A_4 [11]. The most significant feature of the dynamics near an A_l with $l\geqslant 3$ are logarithmic decay laws, where detailed properties have also been worked out in full generality [12]. There are a variety of data indicating that logarithmic decay laws occur in some glass-forming liquids [13–18]. Generically, one has to vary two or three control parameters, respectively, in order to approach these higher-order singularities. It was discovered only recently that the MCT equations for simple systems imply the existence of an A_3 singularity if a hard-sphere repulsion is complemented by a short-ranged attraction shell [19,20]. The A_3 is the end point of a line of A_2 singularities describing glass-to-glass transitions in the parameter plane spanned by the packing fraction φ and the effective attraction strength Γ. At this line there occurs a transition from a glass caused by the cage effect due to the strong repulsion to a glass caused by bond formation due to the dominant role played by the attraction. This transition line extends to low packing fraction and it was argued to be related to the gel transition there [20]. Therefore, this line shall be referred to as *gel* line in the following for the sake of brevity. There is a second transition line that extends to the known transition of the HSS if Γ tends to zero. For brevity, this line shall be referred to as *glass* line in the following. The glass line terminates transversally at the gel line forming a line crossing in the glass-transition diagram. The liquid dynamics close to this crossing shall be studied in this paper.

The existence of a crossing point depends on the attraction to be sufficiently short ranged. If the range δ of the attractive potential increases above a critical value, the glass-glass transition line and the A_3 singularity vanish. This happens in an A_4 singularity as was demonstrated first for the simple system of particles interacting via a square-well potential [21]. The topological singularities A_l are robust against parameter variation. It was shown explicitly for a variety of cases that various interaction potentials or approximation schemes for the static structure factor yield the same qualitative results [21–24]. In this paper, the square-well system (SWS) shall be used as model for the quantitative work. Systems with short-ranged attraction can be realized in colloid-polymer mixtures, where the polymer induces a depletion attraction [25]. Such systems are well under control experimentally and have established thermodynamic

phase behavior [26]. Logically disconnected from the appearance of higher-order singularities, MCT predicts a subtle reentry phenomenon for the glass transitions in such systems [19] which can be related to the variation of the static structure factor [21]. Starting in the glassy state of the HSS and increasing the attraction, the glass is melted for a sufficiently small range of the attraction. Upon further increasing the attraction, the system arrests again. This reentry phenomenon is now firmly established by experiments in colloidal systems [27,28] and by molecular-dynamics simulation [15,28–30].

The scenario suggested by MCT for the A_2 singularity has been applied successfully to analyze experiments and results of computer simulations [31]. It was also applied to systems where both glass and gel transitions occur [14,15,30]. For the dynamics near higher-order singularities, detailed predictions for logarithmic decay and subdiffusive power law in the mean-squared displacement (MSD) have been worked out for the SWS [32]. Indications of logarithmic decay were reported [14] which are compatible with MCT predictions, and a recent study identifies both logarithmic decay in the correlation functions and a subdiffusive power law in the MSD which is consistent with MCT [16]. It is the main objective of the present paper to discuss scenarios in the SWS near a crossing point where the dynamics is influenced by different A_2 singularities and higher-order singularities at once. There are signs of crossing phenomena connected to higher-order singularities in recent experiments with photon correlation spectroscopy in a micellar system [13,17,18], a suspension of poly(methylmethacrylate) (PMMA) colloidal particles [28,33], a system of microgel colloids [27,34], and computer simulation studies [15,28]. For polymers, dielectric measurements could be fitted with scenarios for A_3, A_4 and a line crossing [35–39].

The paper proceeds as follows. Section II introduces the equations of motion of MCT. A comparison of the theoretical glass-transition diagram with the simulation of Ref. [15] in Sec. III motivates the asymptotic analysis which is outlined in Sec. IV and applied to the MSD in Sec. V and to the correlation function in Sec. VI. Section VII presents a conclusion. The Appendix addresses specific questions arising in the numerical determination of the glass-transition singularities.

II. EQUATIONS OF MOTION

All equations of MCT are based on the equations of motion for the normalized density correlators $\phi_q(t) = \langle \rho_{\vec{q}}^*(t)\rho_{\vec{q}}\rangle / \langle |\rho_{\vec{q}}|^2\rangle$ for wave vector $\vec{q}$ and its modulus $q = |\vec{q}|$. When Brownian dynamics for the motion in colloids is assumed, these equations read [1,2,5,40,41]

$$\tau_q \partial_t \phi_q(t) + \phi_q(t) + \int_0^t m_q(t-t')\partial_{t'}\phi_q(t')dt' = 0. \quad (1a)$$

Here, $\tau_q = S_q/(D_0 q^2)$, with D_0 denoting the short-time diffusion coefficient. $S_q = \langle |\rho_{\vec{q}}|^2\rangle$ is the static structure factor of the system. The initial condition is $\phi_q(0) = 1$. The kernel is a bilinear functional of the correlators, $m_q(t) = \mathcal{F}_q[\mathbf{V}, \phi_k(t)]$, with

$$\mathcal{F}_q[\tilde{f}] = \frac{1}{2}\int \frac{d^3k}{(2\pi)^3} V_{\vec{q},\vec{k}} \tilde{f}_k \tilde{f}_{|\vec{q}-\vec{k}|}, \quad (1b)$$

and the vertex $\mathbf{V}$ specified by

$$V_{\vec{q},\vec{k}} = S_q S_k S_{|\vec{q}-\vec{k}|} \rho [\vec{q}\cdot\vec{k} c_k + \vec{q}\cdot(\vec{q}-\vec{k}) c_{|\vec{q}-\vec{k}|}]^2/q^4. \quad (1c)$$

The direct correlation function c_q is connected with S_q by the Ornstein-Zernike relation, $S_q = 1/[1-\rho c_q]$ [42].

The long-time limit of the correlation function, $f_q = \lim_{t\to\infty}\phi_q(t)$, can be calculated from an algebraic equation,

$$f_q/(1-f_q) = \mathcal{F}_q[f], \quad (2)$$

which displays glass-transition singularities when control parameters are varied [2].

For the dynamics of the tagged particle density, $\rho_q^s(t) = \exp[i\vec{q}\cdot\vec{r}_s(t)]$, one obtains similar equations for the correlation function $\phi_q^s(t) = \langle \rho_{\vec{q}}^{s*}(t)\rho_{\vec{q}}^s\rangle$ [1,6],

$$\tau_q^s \partial_t \phi_q^s(t) + \phi_q^s(t) + \int_0^t m_q^s(t-t')\partial_{t'}\phi_q^s(t')dt' = 0. \quad (3a)$$

Here $\vec{r}_s(t)$ denotes the tagged particle position, $\tau_q^s = 1/(D_0^s q^2)$ with the short-time diffusion coefficient for a single particle, denoted by D_0^s. We set $D_0^s = D_0$ in the following. The kernel $m_q^s(t) = \mathcal{F}_q^s[\phi(t), \phi^s(t)]$ is given by the mode-coupling functional for the tagged particle motion,

$$\mathcal{F}_q^s[\tilde{f}, \tilde{f}^s] = \int \frac{d^3k}{(2\pi)^3} S_k \frac{\rho}{q^4} c_k^{s2} (\vec{q}\vec{k})^2 \tilde{f}_k \tilde{f}^s_{|\vec{q}-\vec{k}|}. \quad (3b)$$

For a tagged particle of the same sort as the constituents of the host fluid we can set $c_q^s = c_q$.

The MSD of a tagged particle, $\delta r^2(t) = \langle |\vec{r}_s(t) - \vec{r}_s(0)|^2\rangle$, obeys [6]

$$\delta r^2(t) + D_0^s \int_0^t m^{(0)}(t-t')\delta r^2(t')dt' = 6D_0^s t. \quad (4a)$$

The functional $m^{(0)}(t) = \lim_{q\to 0} m_q^s(t) = \mathcal{F}_{MSD}[\phi(t), \phi^s(t)]$ for the MSD reads

$$\mathcal{F}_{MSD}[\tilde{f}, \tilde{f}^s] = \int \frac{dk}{(6\pi^2)} \rho S_k (c_k^s)^2 \tilde{f}_k \tilde{f}_k^s. \quad (4b)$$

The inverse of this functional determines a characteristic localization length r_s by $r_s^2 = 1/\mathcal{F}_{MSD}[f, f^s]$. The long-time diffusion coefficient D^s can be defined by $\lim_{t\to\infty}\delta r^2(t)/t = 6D^s$ and yields [6]

$$\frac{D_0^s}{D^s} = 1 + D_0^s \int_0^\infty m^{(0)}(t)dt. \quad (5)$$

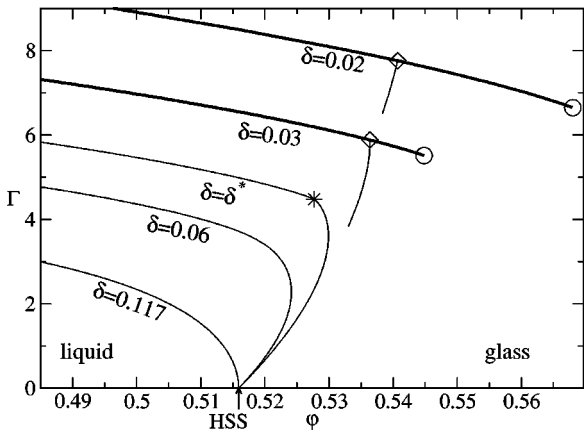

FIG. 1. Glass-transition diagram for the SWS using the structure factor within MSA. Five cuts through the three-dimensional diagram are shown for constant well widths δ as curves for attraction strength Γ vs packing fraction φ. All curves start at the limit of the HSS for $\Gamma=0$ as indicated by the arrow. For $\delta=0.117$ and 0.06 the curves $\varphi^c(\Gamma)$ vary smoothly as Γ is increased. The line $\delta=\delta^*=0.043\,81$ hits the A_4 singularity (*). Curves for $\delta<\delta^*$ exhibit a crossing point ($\diamond$) and an A_3 end point singularity ($\bigcirc$) as demonstrated for $\delta=0.03$ and $\delta=0.02$, where part of the glass-transition line has been erased to avoid cluttering the figure.

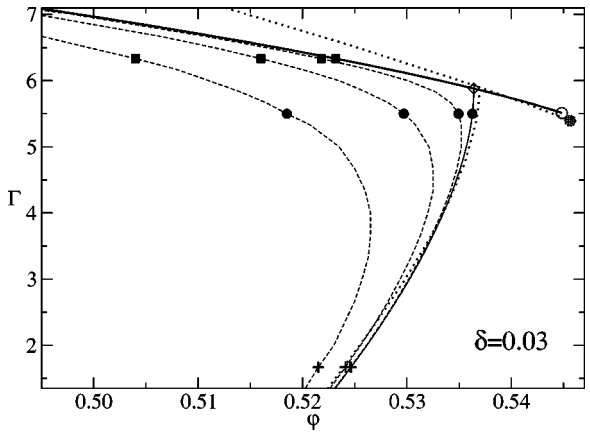

FIG. 2. Glass-transition diagram for the SWS at $\delta=0.03$ (full lines) together with isodiffusivity lines for $D_0^s/D^s=10^5,10^7,10^{10}$ (dashed lines, from left to right) based on the structure factor using MSA. The A_3 singularity is indicated by a circle ($\bigcirc$) and a crossing point by a diamond ($\diamond$). On the isodiffusivity lines, states are marked for $\Gamma=1.67$ (+), 5.50(●), and 6.33(■). The dotted lines with the shaded circle as end point show the glass-transition singularities for $\delta=0.03$ based on the structure factor using PYA rescaled in Γ by a factor 5.88 to match the crossing point.

For the equations above, the static structure factor S_q is required as input, which can be calculated from the interaction potential after some closure relation is invoked [42]. For SWS, we use an approximate analytical solution of the mean-spherical approximation (MSA) and a numerical solution to the Percus-Yevick approximation (PYA) [21]. The SWS consists of N particles in a volume V at density $\rho=N/V$ with hard-core diameter d and an attractive well of depth u_0 and width Δ. We describe the SWS by three dimensionless control parameters: the packing fraction $\varphi=d^3\rho\pi/6$, the attraction strength $\Gamma=u_0/(k_BT)$, and the relative well width $\delta=\Delta/d$. The unit of length is chosen to be $d=1$. The unit of time is chosen so that $D_0=1/160$. Wave-vector space shall be discretized to M grid points with spacing $\Delta q=0.4$ and a cutoff $q^{\max}$ large enough to assert convergence of the integral in Eq. (1b) for the long-time limit. The procedures for the numerical solution of Eqs. (1) to (5) have been outlined previously [32,43,44]. Asymptotic laws close to the singularities are presented in the Appendix, which allow for accurate and fast determination of both A_3 end points and glass-glass transition points.

III. GLASS-TRANSITION DIAGRAMS

The three-dimensional control-parameter space for the SWS can be examined by considering cuts through the set of glass-transition singularities for constant δ. In each plane the transition points are calculated by finding the bifurcation points of Eq. (2). Figure 1 displays the singularities for several cuts. The glass-transition diagram is organized around the A_4 singularity (* in Fig. 1) at $(\varphi^*,\Gamma^*,\delta^*)^{\mathrm{MSA}}=(0.5277,4.476,0.043\,81)$. From there emerge for $\delta<\delta^*$ both the line of A_3 end points, ($\bigcirc$ in Fig. 1) $[\varphi^\circ(\delta),\Gamma^\circ(\delta)]$, and the line crossings ($\diamond$ in Fig. 1) $[\varphi^\diamond(\delta),\Gamma^\diamond(\delta)]$, separating glass transitions for $\Gamma<\Gamma^\diamond$ from gel transitions for $\Gamma\geqslant\Gamma^\diamond$. The line of gel transitions extends beyond the crossing point into the arrested state as glass-glass-transition line and terminates at the A_3 singularity. For $\delta>\delta^*$, glass- and gel-transition lines join smoothly as seen for $\delta=0.06$ and 0.117. For $\delta<\delta_{\mathrm{reentry}}$ the lines of glass transitions display the reentry phenomenon discussed above. At $\delta=\delta_{\mathrm{reentry}}$ this reentry disappears [24]. When using the analytical result for S_q in MSA we get $\delta_{\mathrm{reentry}}^{\mathrm{MSA}}=0.117$, while for the PYA one finds the larger value $\delta_{\mathrm{reentry}}^{\mathrm{PYA}}=0.145$. To assure that the smaller value for the MSA is not caused by the expansion in δ used for the calculation of S_q, we determine $\delta_{\mathrm{reentry}}$ again, this time solving the MSA numerically. This yields $\delta_{\mathrm{reentry}}^{\mathrm{MSA}}=0.112$. Therefore the deviation between the MSA and PYA results has to be understood as a difference in the way the closure relations incorporate the subtle changes in S_q that lead to the reentry as explained earlier [21].

For the discussion of the crossing we choose the cut $\delta=0.03$ from Fig. 1 which is shown in Fig. 2 as full line. The ratio of the diffusivity D^s compared to the short-time diffusion coefficient D_0^s can be used to characterize the distance of a chosen state to the liquid-glass-transition line. The dashed lines in Fig. 2 show states for constant D_0^s/D^s with D^s defined in Eq. (5). These lines are plotted for the cut $\delta=0.03$ also using the MSA for the evaluation of the structure factor. These isodiffusivity lines can be interpreted as approximations of the liquid-glass-transition line. They also display the reentry phenomenon as discussed above. The liquid-glass-transition line follows closely the isodiffusivity curves but is separated further from them around the crossing point. This indicates the influence of more than one singularity on the dynamics in that region. If the PYA instead of the MSA is used to calculate the structure factor input, the dotted lines of liquid-glass- and glass-glass-transition curves are

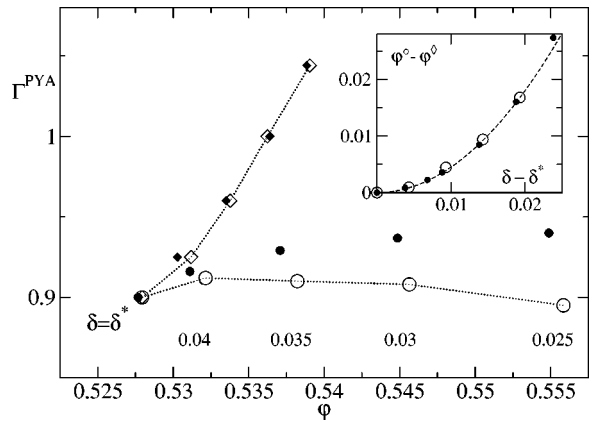

FIG. 3. End points (○) and crossing points (◇) for the SWS in PYA for $\delta=\delta^*$, 0.04, 0.035, 0.03, 0.025. The crossing points based on the MSA can be scaled on top of the PYA result by a δ-dependent prefactor, $\Gamma^{\mathrm{PYA}}=y(\delta)\Gamma^{\mathrm{MSA}}$ with $y(\delta)\approx 0.1+2.34\delta$. Crossing points and end points based on the MSA are shown by filled symbols. The inset shows the difference in φ between crossing points and end points for increasing $\delta^*-\delta$. Results for the PYA and the MSA are shown by open and filled symbols, respectively. The dashed curve displays the fit $\varphi^*-\varphi^{\diamond}=45(\delta^*-\delta)^2$.

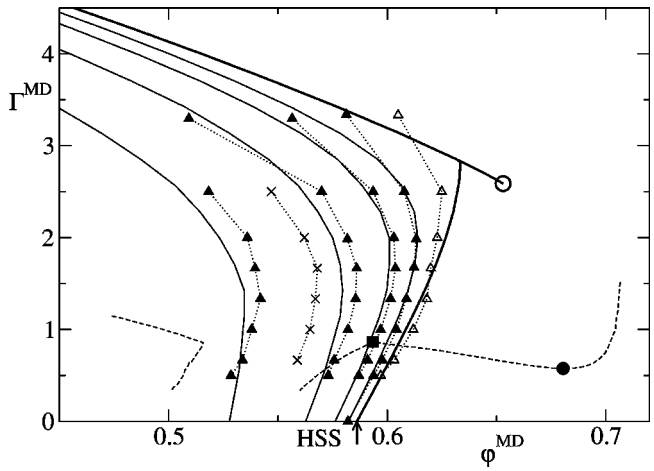

FIG. 4. Results for the SWS for $\delta=0.03$. Triangles (▲) mark the isodiffusivity curves from the simulation in Ref. [15] from left to right for $D_0^s/D^s=2\times10^2$, 2×10^3, 2×10^4, 2×10^5, respectively. Open triangles △ indicate the extrapolation of the diffusivity data [16]. Crosses (×) show the isodiffusivity curve for $D_0^s/D^s=2.4\times10^2$ from the simulation of the monodisperse system [29]. Dotted lines are guides to the eye for the data from MD simulation. Dashed lines indicate the data for melting, freezing, and solid-solid binodal together with the solid-solid triple point (■) and critical point (●) from Ref. [45]. Full lines are theoretical calculations using the PYA structure factor for liquid-glass transitions, the glass-glass transition with end point A_3 (○) and the respective isodiffusivity curves for $D_0^s/D^s=2\times10^2,2\times10^3,2\times10^4,2\times10^5$ (from left to right). The arrow labeled HSS indicates the limit of the hard-sphere system from Ref. [15]. The MCT results are based on the PYA and the control parameters φ^{PYA} and Γ^{PYA} are transformed by $\varphi^{\mathrm{MD}}=2.25\varphi^{\mathrm{PYA}}-0.5747$ and $\Gamma^{\mathrm{MD}}=2.85\Gamma^{\mathrm{PYA}}$ to match the isodiffusivity curves from the simulation.

found. The result for both closure relations can be matched reasonably at the crossing point by only rescaling Γ by a factor of 5.88. The agreement for the almost horizontal gel-transition lines is less satisfactory but the glass-transition lines almost fall on top of each other. As noted in the preceding paragraph, the reentry is more pronounced for the result using the PYA than for the MSA. The different packing fractions at the crossing are $\varphi^{\diamond}_{\mathrm{MSA}}=0.5364$ and $\varphi^{\diamond}_{\mathrm{PYA}}=0.5362$, while the difference in the location of the A_3 singularities is slightly larger, $\varphi^{\bigcirc}_{\mathrm{MSA}}=0.5449$ and $\varphi^{\bigcirc}_{\mathrm{PYA}}=0.5456$.

Figure 3 shows the A_3 singularities and the crossing points when using S_q in PYA (empty symbols). Matching the crossing points from the result using the MSA, cf. Fig. 1, again by multiplications in Γ, yields good agreement in $\varphi^{\diamond}$ for all values of δ. After the transformation, the A_3 singularities for a given δ differ in Γ by 5% and less, while the deviations in φ are comparable to those found for the crossings. It should be noted that all end points are found at roughly the same attraction strength, $\Gamma\approx0.9$, whereas the crossing points move to higher Γ as the well width is decreased. At the A_4 singularity, the end point absorbs the crossing point, and the difference $\varphi^*-\varphi^{\diamond}$ approaches zero in a minimum. Therefore, crossing point and end point separate from each other quadratically when close to the A_4 singularity. This is demonstrated in the inset of Fig. 3 for the results using both MSA and PYA as input, respectively.

One cannot expect a theory for a singularity to predict accurate numbers for the control parameters of the singularities. For that reason the distance from the singularity should be used for a comparison of the theoretical results with data from experiments or computer simulation. The isodiffusivity curves in Fig. 2 motivate a comparison between MCT and computer simulation based on the ratio D_0^s/D^s [15]. Figure 4 shows that an acceptable fit of data for the diffusivity in Ref. [15] and the theoretical data calculated using the structure factor evaluated in PYA is achieved by keeping the well width fixed at $\delta=0.03$ and scaling the axis of the inverse temperature by $\Gamma^{\mathrm{MD}}=2.85\Gamma^{\mathrm{PYA}}$. This preserves the limiting case of the HSS as done above for the comparison of PYA and MSA, cf. Fig. 2. Trying to match reasonably at least the two curves with the highest ratio of D_0^s/D^s, the packing fraction has to be taken $\varphi^{\mathrm{MD}}=2.25\ \varphi^{\mathrm{PYA}}-0.5747$ in order to keep a value for HSS of $\varphi^c_{\mathrm{HSS}}=0.586$. This is consistent with the diffusivity data and experiments done in colloids [8,9]. The prefactor of 2.25 seems somewhat large and it is already seen in Fig. 4 that this overestimates the differences in φ further from the singularities. But taking the diffusivity data for granted, this large prefactor is required. A modification of the third coupling parameter δ was not necessary in the fit.

Figure 4 demonstrates a reasonable fit between theory and data starting from the HSS and extending up to the crossing point. For the gel transitions, there are not enough data available to make a definite statement. For this high value of Γ it is also difficult to obtain accurate values for D^s with good statistics from the simulation [15]. These points are only fitted qualitatively in Fig. 4. An extrapolation of the diffusivity data was used in Ref. [16] to determine the open triangles that represent a different estimate for the liquid-glass transi-

tion line. These points agree well with the transformed theoretical curves but tend to deviate closer to the crossing. A comparison of the fit in Fig. 4, which uses the PYA for the theoretical curves, with Fig. 2 indicates that using MSA for the structure factor would also properly fit the data from the HSS limit up to the crossing but would be worse than PYA for the gel line. The indication of the A_3 singularity in Fig. 4 has to be understood as an extrapolation of the transformation scheme outlined above. A slight reservation has to be made since the simulation data refer to a binary mixture while the present theory deals with a monodisperse system. However, comparing the data from the simulation of the monodisperse case [29] indicated by crosses in Fig. 4 with the ones for the mixture, the isodiffusivity for $D_0^s/D^s=2.4\times10^2$ seems to fit nicely into the picture. Data for lower D_0^s/D^s from Ref. [29] have the same trend in Γ but apparently do not occur at control parameter values for the same diffusivity as extrapolated from the mixture. The MD studies were performed using Newtonian dynamics where an appropriate definition of D_0^s is impossible; the value $d\sqrt{k_BT/m}$ is taken instead of D_0^s as reference which introduces a reasonable microscopic time scale [15,29]. This problem in the definition of the analog of D_0^s introduces less deviations for larger ratios of the diffusivity D_0^s/D^s since only the order of magnitude is important for the definition of the isodiffusivity curves. A deviation in $\log D_0^s$ would stay the same for both large and small differences in $\log D_0^s-\log D^s$ and the result can be more accurate the larger the ratio D_0^s/D^s is. Therefore, putting emphasis on the data with high ratios of D_0^s/D^s is justified.

The fit in Fig. 4 shows that, in general, MCT overestimates the trend to freezing when coupling parameters are increased. This was already found for the HSS [8] and a binary Lennard-Jones mixture [46]. Yet, for a Lennard-Jones potential the mechanism of arrest is still dominated by repulsion, so the control parameter is effectively only density also in that system. For the SWS near the line crossing, necessarily both mechanisms of arrest have to be of the same importance and the approximation inherent to MCT has to preserve the relative importance of both mechanisms. In the case of the SWS, MCT has apparently the same tendency in the error for the treatment of couplings in φ and Γ. The mapping of the theoretical results to *higher* experimental values of both packing fraction and attraction strength is also in agreement with a recent experimental analysis of a colloid-polymer mixture with the theoretical results for the Asakura-Oosawa potential [47]. For the latter work, a qualitatively similar mapping could be suggested to match experiments and theoretical predictions. By comparison with the data for the phase transitions [45] in Fig. 4, we recognize that the crossing of lines and the A_3 singularity are located in the metastable region with respect to the solid-solid binodal. The A_3 singularity differs by 4% in φ and by a factor of 4.5 in Γ from the solid-solid critical point.

IV. ASYMPTOTIC EXPANSIONS

For the description of the dynamics at the crossing, asymptotic expansions at the two different singularities shall be applied with the separation from the respective singularity as small parameter. The separations from an A_2 or A_3 singularity shall be denoted by σ and ε, respectively. The expansions for A_2 singularities which are valid for glass-, gel- and glass-glass-transition points are taken from Refs. [5,6], the expansions for the A_3 singularity are found in Refs. [12,32]. Only those formulas which are needed below are compiled in the following. For both A_2 and A_3 singularities the expansion for the density correlation function can be stated in the general form

$$\phi_q(t)=f_q^c+\hat{f}_q+h_q\{G(t)+[H(t)+K_qG(t)^2]\}, \qquad (6)$$

where the plateau correction $\hat{f}_q$ and the terms in square brackets are of next-to-leading-order. Neglecting these terms leaves the leading order result, $\phi_q(t)=f_q^c+h_qG(t)$, which comprises the factorization theorem of MCT [2], stating that the deviation of $\phi_q(t)$ from the plateau f_q^c factorizes into time-dependent function $G(t)$ and a critical amplitude h_q. This factorization is violated in next-to-leading order by $\hat{f}_q$ and the term $K_qG(t)^2$ with the correction amplitude K_q. While the general formulas for f_q^c, h_q and K_q are the same for the expansions at both singularities, $G(t)$, $H(t)$, and $\hat{f}_q$ are specific for the particular expansion. At an A_2 singularity the leading-order result is given by the β-correlation function [2],

$$G(t)=\sqrt{|\sigma|}g_\lambda^{\pm}(t/t_\sigma), \quad t_\sigma=t_0/|\sigma|^{1/2a}, \quad \sigma\gtrless0, \qquad (7)$$

where the lower signs refer to the weak coupling side of the transition. The overall time scale t_0 is used as fit parameter. For $\sigma=0$, the above formula simplifies to a power law as does the correction,

$$G(t)=(t_0/t)^a, \quad H(t)=\kappa(a)(t_0/t)^{2a}, \qquad (8)$$

with a function $\kappa(x)$,

$$\kappa(x)=[\xi\Gamma(1-3x)-\zeta\Gamma(1-x)^3]/[\Gamma(1-x)\Gamma(1-2x)-\lambda\Gamma(1-3x)]. \qquad (9)$$

Here, $\Gamma(x)$ denotes the Gamma function and λ is the exponent parameter, $\lambda=\Gamma(1-a)^2/\Gamma(1-2a)$. For an A_2 singularity, $0.5\leqslant\lambda<1$, while $\lambda=1$ specifies an A_3 singularity. Formulas for the parameters ξ and ζ are found in Ref. [5].

For the MSD, the analog of Eq. (6) reads [6,32]

$$\delta r^2(t)/6=r_s^{c2}-\hat{r}_s^2-h_{\mathrm{MSD}}\{G(t)+[H(t)+K_{\mathrm{MSD}}G(t)^2]\}, \qquad (10)$$

where only the plateau correction $\hat{r}_s^2$ is again specific to the expansion considered. Inserting Eq. (8) into Eq. (10) yields the following form for the description of the MSD at the A_2 transition point [6],

$$\delta r^2(t)/6=r_s^{c2}-h_{\mathrm{MSD}}(t_0/t)^a\{1+[K_{\mathrm{MSD}}+\kappa(a)](t_0/t)^a\}. \qquad (11)$$

The increase of the MSD above the plateau r_s^{c2} is given by the von Schweidler law,

$$\delta r^2(t)/6 = r_s^{c2} + h_{\rm MSD}(t/t'_\sigma)^b\{1-[K_{\rm MSD}+\kappa(-b)](t/t'_\sigma)^b\}, \tag{12}$$

with $\Gamma(1+b)^2/\Gamma(1+2b)=\lambda$. The time scale t'_σ obeys another power-law scaling, $t'_\sigma = t_0/(B^{1/b}|\sigma|^\gamma)$, $\gamma = 1/(2a) + 1/(2b)$, where the number B is tabulated in Ref. [48].

The leading-order result for an A_3 singularity is given by

$$G(t) = -B\ln(t/\tau), \quad B=\sqrt{[-6\varepsilon_1/\pi^2]}, \tag{13}$$

where the time scale τ is used to match the asymptotic description with the solution. The corrections in Eqs. (6) and (10) are completed by specifying

$$H(t) = \sum_{i=1}^{4} B_i \ln^i(t/\tau). \tag{14}$$

The definitions for $\hat{f}_q$, $\hat{r}_s^2$ at the A_3 singularity and the parameters B, B_i, and ε_1 are found in Ref. [12]. The solution for the MSD at an A_3 singularity can be represented in an alternative form as a power law [32],

$$\delta r^2(t)/6 = r_s^{c2}(t/\tau)^x, \tag{15a}$$

with exponent

$$x = h_{\rm MSD}B/r_s^{c2}. \tag{15b}$$

The next-to-leading-order result implies a correction to the exponent

$$x' = h_{\rm MSD}(B-B_1)/r_s^{c2}. \tag{16a}$$

and reads

$$\delta r^2(t)/6 = (t/\tau)^{x'}\{r_s^{c2} - \hat{r}_s^2 + b_2 r_s^{c2}\ln(t/\tau)^2 + a_3\ln(t/\tau)^3 + a_4\ln(t/\tau)^4\}. \tag{16b}$$

Here $b_2 = (2r_s^{c2}a_2 - a_1^2)/(2r_s^{c4})$, $a_1 = h_{\rm MSD}(B-B_1)$, $a_2 = -h_{\rm MSD}(B_2 + K_{\rm MSD}B^2)$, $a_3 = -h_{\rm MSD}B_3$, and $a_4 = -h_{\rm MSD}B_4$.

V. RESULTS FOR THE MEAN-SQUARED DISPLACEMENT

Three paths are marked in Fig. 2 for the discussion of the dynamics. The first path for $\Gamma = 1.67$ is relatively far from the crossing point and is connected to a glass transition. The path for $\Gamma = 5.50$ is close to but below the crossing point and close to the A_3 singularity. The third path is connected to a gel transition beyond the crossing point. All paths end at an A_2 singularity given by the respective Γ. The changes in the MSD when approaching the different liquid-glass-transition points shall be analyzed using the asymptotic laws for the A_2 singularity in the following. The asymptotic laws for the critical relaxation at A_2 singularities from Eq. (11) are compared with the full MCT result in Fig. 5. For $\Gamma = 1.67$ [Fig. 5(a)] the description is similar to that found for the HSS [6].

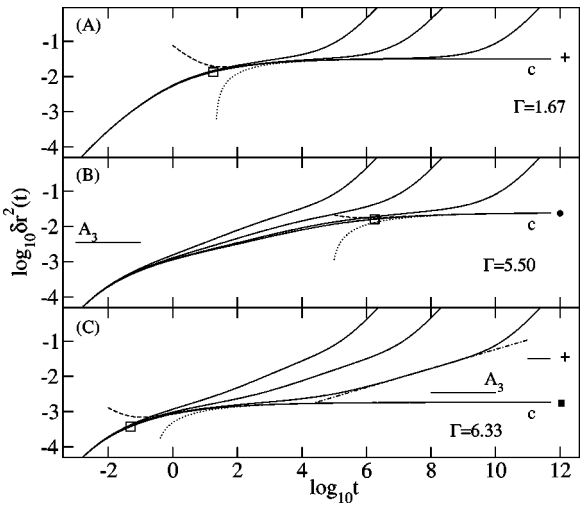

FIG. 5. MSD for the SWS at the crossing. Full curves are the results for states on the isodiffusivity lines for $D_0^s/D^s = 10^5, 10^7, 10^{10}$ marked in Fig. 2. The curves with label *c* refer to the transition points for the value of Γ indicated. Respective values for the plateaus $6r_s^{c2}$ are marked by the symbols +, ●, and ■ introduced in Fig. 2. In the lower two panels, the plateau for the A_3 singularity is shown as horizontal line. Dotted curves show the leading solution to the critical law, $(t_0/t)^a$, dashed curves the next-to-leading order for the A_2 singularities, Eq. (11). Open squares (□) denote the time where the solution deviates by 20% from the asymptotic result in Eq. (11). An effective power law for exponent $\tilde{x}=0.27$ appearing at $\Gamma=6.63$ is shown by the dash-dotted line (see text). Here and in the following figures the unit of length is the hard core diameter $d=1$.

The exponent parameter $\lambda^{\rm A}=0.750$ is still close to the one for the HSS, $\lambda=0.735$. But the time scale $t_0^{\rm A}=1.95$ differs considerably from the value $t_0=0.425$ for the HSS. This is due to a slowing down of the dynamics for times where $\delta r^2(t)$ is smaller than r_s^{c2} caused by the attractive forces on smaller length scale. The exponent for the critical relaxation is $a=0.305$. The point where the description by Eq. (11) and the numerical solution deviate by 20% of the critical plateau value $6r_s^{c2}$ is marked by a square at $t\approx 18\approx 9t_0$.

Figure 5(b) shows the scenario for an approach to an A_2 singularity on the path closer to the A_3 singularity. The exponent parameter is increased to $\lambda^{\rm B}=0.857$ corresponding to a decrease of the critical exponent to $a=0.243$. The increasing importance of the attraction is seen in a decrease of the critical localization length representing the plateaus for the MSD from $6\,r_s^{c2}=0.0318$ [labeled by + in Fig. 5(a)] to $6\,r_s^{c2}=0.0245$ [marked by ● in Fig. 5(b)]. However, the major new phenomenon is the drastic increase of the time scale t_0 to $t_0^{\rm B}=4\times 10^3$. The critical decay for the A_2 singularity sets in only for times around $t\approx 10^6$ as indicated by the square in Fig. 5(b). There is an additional relaxation process outside the transient ruling the dynamics within the window $0\leqslant \log_{10}(t)\leqslant 4.5$. The critical localization length of the nearby gel transition yields $\delta r^2\approx 10^{-3}$. Therefore, the anomalous decay process is not the one related to the gel transition. Rather, it is the decay around the plateau of the close-by A_3 singularity which appears as a subdiffusive re-

gime with almost power-law-like variation. This later phenomenon shall be explained in detail below.

In Fig. 5(c) for $\Gamma=6.33$, the gel plateau is approached with $t_0=6\times10^{-3}$ and the critical relaxation for $\lambda^C=0.873$ and $a=0.232$ is described with similar accuracy as discussed in Fig. 5(a). The deviation of 20% is at $t=0.048=8t_0$ and again indicated by a square. The comparably large value of λ causes the leading asymptotic approximation (dotted curve) to deviate further from the next-to-leading order result. The amplitude $[K_{\mathrm{MSD}}+\kappa(a)]$ in Eq. (11) is around -1 in Figs. 5(a) and 5(c). In this sense, one concludes that the critical dynamics for the gel transition is quite similar to the one observed for the glass transition.

The dynamics for the $\delta r^2(t)$ exceeding the respective plateaus is quite different for the glass transition shown in Fig. 5(a) from the gel transition in Fig. 5(b). Let us, as usual, refer to the process with $\delta r^2(t)>6r_s^{c2}$ as an α process. The α process shown in Fig. 5(a) is similar to the one in the HSS. The crossing of the plateau is followed by a von Schweidler relaxation and a crossover to long-time diffusion [6]. A rescaling of the time can condense the curves on top of each other, a property known as α scaling. For the dynamics at the gel transition shown in Fig. 5(c), the lower plateau (■) defines the onset of the α process. The shape of the $\log\delta r^2$-versus-$\log t$ curve differs qualitatively from the one shown in Fig. 5(a). The relaxation around the A_3 singularity plateau causes effective power-law behavior with $\tilde{x}=0.27$ as shown by the dash-dotted line. It is the same phenomenon as observed above in Fig. 5(b). On approaching the gel transition, this subdiffusive regime scales as part of the α process. This holds if the distances to neither the nearby glass transition nor the A_3 singularity are seriously altered as we further approach the gel transition. Under this condition, the A_3 singularity and the glass-transition singularity influence only the shape of the α-relaxation curves. On the other hand, if the distance between the glass transition and the A_3 singularity is changed on the path taken, the form of the α process is also modified. In this case, the A_3 singularity is manifested in a violation of the α scaling for the gel transition as found in a recent simulation study [14]. If the separation from the A_3 singularity and the glass-transition singularity is sufficiently large, which is true for small φ, the dynamics is affected only by the gel plateau and directly crosses over from the von Schweidler relaxation at the gel plateau to the long-time diffusion. For this reason, the exponent $\tilde{x}$ of the effective power law approaches unity upon increasing Γ.

Figure 6 shows the parameters for the asymptotic description via Eq. (11) as a function of Γ along the liquid-glass-transition lines for $\delta=0.03$. The localization lengths r_s^c in Fig. 6(a) exhibit a jump at the crossing point $\Gamma^\diamond$ reflecting the discontinuous change of f_q^c. The values for the glass-glass transition are also shown down to the A_3 singularity at Γ°. The critical amplitudes h_{MSD} follow the same trend as r_s^c, signaling that a change in the localization length also sets the amplitude for the relaxation around r_s^c. Figure 6(b) shows the two quantities in the correction to the critical law. K_{MSD} shows only small deviations from the value in the HSS, $K_{\mathrm{MSD}}^{\mathrm{HSS}}=-1.23$. On the glass line at the crossing,

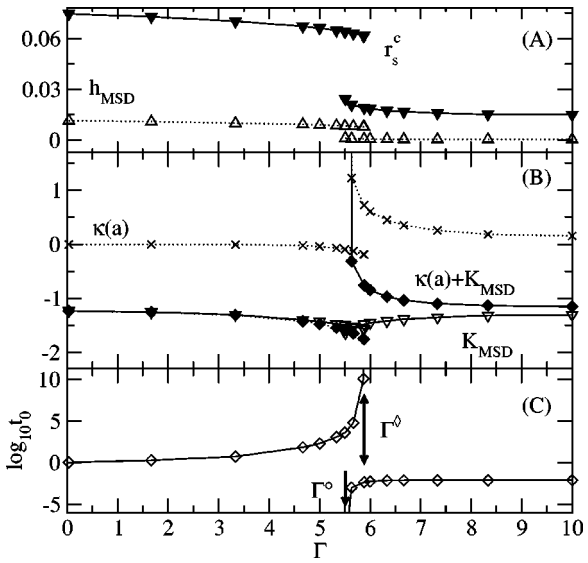

FIG. 6. Parameters for the critical decay at A_2 singularities according to Eq. (11); r_s^c (▼) and h_{MSD} (△) in panel (a); $\kappa(a)$ (×) from Eq. (9), K_{MSD} (▽), and $\kappa(a)+K_{\mathrm{MSD}}$ (◆) in panel (b); and t_0 (◇) in panel (c). The arrow labeled Γ° marks the value for the A_3 singularity, $\Gamma^\diamond$ the crossing point. Full and dotted lines are guides to the eye to join points on different parts of the glass-transition line for $0\leqslant\Gamma\leqslant\Gamma^\diamond$ and the gel-transition line for $\Gamma^\circ\leqslant\Gamma$, respectively.

$K_{\mathrm{MSD}}=-1.57$, and on the gel line it reaches $K_{\mathrm{MSD}}=-1.31$. At the A_3 singularity, $K_{\mathrm{MSD}}=-1.64$. Since away from crossing and higher-order singularities, $\kappa(a)$ is always close to zero, the correction to the critical law in Eq. (11) is dominated by the amplitude K_{MSD} which is negative and of order unity there. For this reason, including the correction to the critical law in Fig. 5 increases the range of applicability considerably in comparison to the leading approximation. At higher-order singularities, $\lambda\to1$, and $\kappa(a)$ diverges. This is responsible for the increase of the corrections at the crossing. These corrections change sign when $\kappa(a)$ starts to increase. For the case of $\delta=0.03$, this happens only on the glass-glass-transition line between Γ° and $\Gamma^\diamond$.

Figure 6(c) points out the difference in the time scale t_0 when coming from small Γ in the HSS limit or from high Γ, respectively. In the first case, t_0 for the critical law at the glass-transition plateau is increasing and eventually diverging when the gel transition at the crossing is approached. This is because the glassy dynamics of the gel transition determines t_0. For $\Gamma>\Gamma^\circ$, t_0 is orders of magnitude smaller than in the HSS since the relevant localization for the gel is encountered much earlier in time. On this line of transitions, t_0 is regular at the crossing but diverges at the A_3 singularity. This indicates that power laws are an inadequate description of the critical relaxation at a higher-order singularity.

Figure 7 displays the parameters quantifying the von Schweidler approximation in Eq. (12). Figure 7(a) refers to states on the isodiffusivity line $D_0^s/D^s=10^{10}$ in Fig. 2. The isodiffusivity lines bend away from the crossing and this translates into the separation parameters $|\sigma|$ being maximal there. On the same curve, the separation from the A_3 singu-

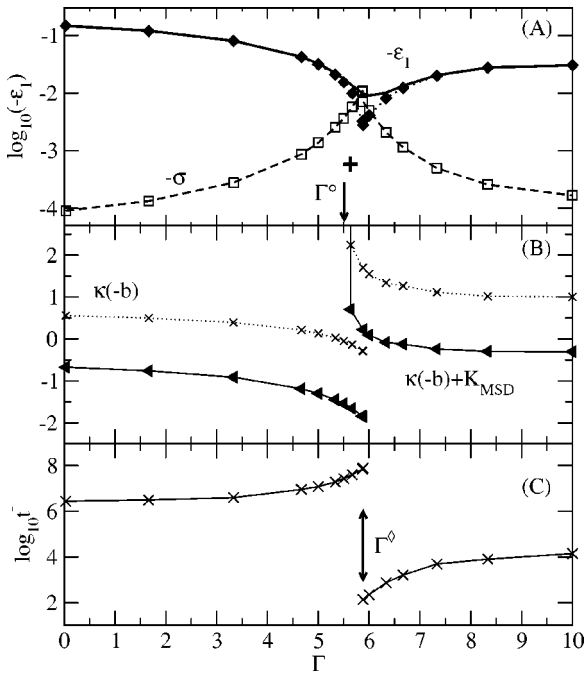

FIG. 7. Parameters for the von Schweidler law description, Eq. (12), for $\delta=0.03$. Panel (A) shows the separation parameters σ for points on the isodiffusivity line for $D_0^s/D^s=10^{10}$ ($\square-\square$). The separation of the same points from the A_3 singularity, ε_1, is shown by the full line. The separation ε_1 of points on the liquid-glass transition for given Γ is shown by filled symbols ($\blacklozenge\cdots\blacklozenge$), the plus symbol marks ε_1 for the glass-glass transition for $\Gamma=5.63$. panel (b) exhibits the amplitudes of the correction in Eq. (12), $\kappa(-b)+K_{\mathrm{MSD}}$ ($\blacktriangleleft$) and $\kappa(-b)$ ($\times$), cf. Eq. (9). The values for K_{MSD} are the same as shown in Fig. 6. panel (c) shows the time t^- where the respective critical A_2 plateau is crossed by the MSD for $D_0^s/D^s=10^{10}$.

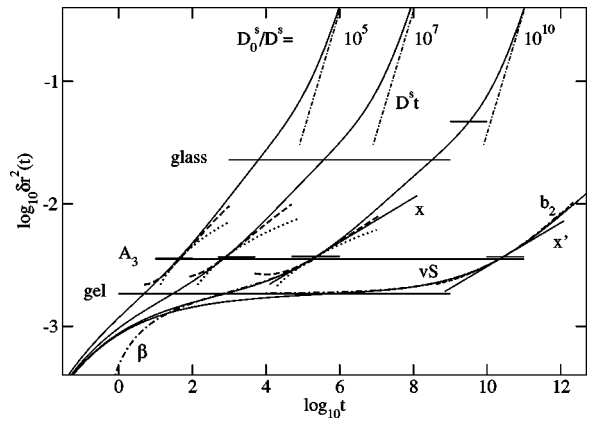

FIG. 8. Asymptotic description of the MSD near the A_3 singularity. The full lines are the MSD for states with $\Gamma=6.33$ and increasing φ. Three curves reproduce the results from Fig. 5(c) and the last one refers to $\varphi=0.5231$. The long horizontal lines show the critical plateaus $6r_s^{c2}$ for the gel transition at $\Gamma=6.33$, the A_3 singularity and the glass transition at the crossing point for $\Gamma=5.88$. The short horizontal lines indicate the corrected plateau $6(r_s^{c2}-\hat{r}_s^2)$ for the asymptotic laws associated with the respective relaxation. The β-relaxation asymptote around the gel plateau, Eq. (7) , is drawn as a chain curve labeled β for the solution at $D_0^s/D^s=10^{10}$ (compare text). The chain line labeled vS represents the von Schweidler description for the state at $\varphi=0.5231$. For $D_0^s/D^s=10^5$, 10^7, and 10^{10} dotted and dashed lines show the leading and next-to-leading approximation near the A_3 plateau in Eq. (10), respectively. The straight full line labeled x shows the approximation by Eq. (15a), x' the corrected power law (16a), and the dashed line labeled b_2 the approximation by Eq. (16b). The straight dash-dotted lines show the asymptotic long-time diffusion D^st for the respective curves.

larity $|\varepsilon_1|$ has a minimum around the crossing. This also shows that distances in control-parameter space as apparent, e.g., in Fig. 2 need not necessarily reflect the relevant separation parameters of the singularity for the asymptotic description. The difference in coordinates of the liquid-glass-transition point for $\Gamma=5.50$ from the A_3 is $(\Delta\phi,\Delta\Gamma)=(0.085, 0.01)$ while for the crossing point $(\Delta\phi,\Delta\Gamma)=(0.084, -0.37)$. This would suggest that the former point is closer to the A_3 than the crossing point. The separation parameters, however, are $\varepsilon_1=-0.028$ and -0.015, respectively, indicating that the influence of the A_3 singularity on the crossing is stronger. Figure 7(b) displays the correction amplitudes in Eq. (12). K_{MSD} is the same as in Fig. 6 and $\kappa(-b)$ shows similar behavior as $\kappa(a)$ in Fig. 6. However, as $\kappa(-b)$ is larger than $\kappa(a)$ on the gel line it almost compensates the negative values of K_{MSD} and $K_{\mathrm{MSD}}+\kappa(-b)$ is close to zero.

The time t^- for the onset of the α process, i.e., the time where the critical plateau is crossed, is shown in Fig. 7(c). When the long-time diffusion is given by the ratio $D_0^s/D^s=10^{10}$, the plateau in the localization is encountered by the MSD for the HSS at $t^-=3\times10^6$. This is the time when the cage around a tagged particle disintegrates and the particle starts to diffuse. The increasing attraction for $\Gamma>0$ introduces short-ranged bonding among the particles before the particles experience the cage. Hence, for the same reason as for the increase of t_0, this bonding process shifts t^- to higher values. When comparing the lower panels of Figs. 6 and 7 we observe that for $0\leqslant\Gamma\leqslant5$, the time scales t_0 and t^- run almost parallel and define a window of six orders of magnitude in time where the cage effect dominates the dynamics. For large coupling, $\Gamma\geqslant8$, we observe a comparable window for the dynamics around the gel plateau, where bonding rules the dynamics. Therefore, in both cases the stretching of the dynamics is the same as is corroborated by observing that $\lambda\lesssim0.8$ in the mentioned regions [21]. In this sense, also the α processes of glass- and gel-transition singularities are similar if one is unaffected by the other. For $5\lesssim\Gamma\lesssim7$, or $\lambda\gtrsim0.8$, the dynamics is governed by the interference of both mechanisms and the emergence of the A_3 singularity.

Figure 8 shows the asymptotic approximation of the α process for states with $\Gamma=6.67$ and increasing φ, cf. Fig. 2. Three plateaus organize the relaxation. First, the gel plateau is encountered. Shown here as dash-dotted curve labeled β is the first-order description by the full β-correlation function from Eq. (7). It continues the description by the critical law discussed in Fig. 5. The correction in Eq. (12) for that A_2 singularity is close to zero as for almost all gel transitions for $\delta=0.03$, cf. Fig. 7. This explains why the first-order description is so successful in the regime after crossing the plateau.

After the plateau, the curve for the β correlator cannot be discerned from the full solution. It extends, accidentally, also beyond the region of applicability which is limited by the A_3 plateau. To demonstrate that upon closer approaching the A_2 singularity for the gel transition, the α scaling picture from Fig. 5(a) reemerges, we show an additional relaxation for $\varphi=0.5231$. This has a similar separation parameter, $\sigma=-10^{-4}$, as the curve $D_0^s/D^s=10^{10}$ in Fig. 5(a). This last curve in Fig. 8 clearly displays the two-step relaxation and is described well by the von Schweidler law (12).

The second plateau is associated with the logarithmic relaxation laws. The curvature of the log δr^2-versus-log t curve is positive around the plateau and therefore the leading approximation, Eq. (13), which implies negative curvature, disagrees qualitatively. Including the corrections in Eq. (10) with $H(t)$ given by Eq. (14), one gets the dashed lines. These describe two decades in time for all curves shown when requiring 5% accuracy. The asymptotic laws for the A_3 singularity describe approximately half of the relaxation between the gel and the glass plateau. In particular, the onset of the effective power law discussed in Fig. 5 is captured by the asymptotic approximation. However, the range of applicability for the logarithmic laws is bound by the neighboring plateaus for gel and glass transitions. For this reason, the approximations for the A_3 singularity do not extend beyond the range shown in the figure. In particular, the effective power law with exponent $\tilde{x}$ is explained only in the first part by the logarithmic laws and is continued by a crossover to the dynamics at the plateau of the glass transition.

To differentiate the effective power law from the power laws discussed for the MSD in Ref. [32], we show the latter for comparison as dotted line in Fig. 8. Let us note first that for all states considered we find $b_2>0$. The approximation by the leading-order power law (15a) describes one and a half decades on the 5% level as seen for the curve $D_0^s/D^s=10^{10}$. The exponents capture the diminishing slope upon approaching the A_3 singularity by decreasing from left to right, $x=0.331$, 0.243, 0.181, 0.163. The corrected power law, Eq. (16a), yields an exponent $x'=0.178$ for the last relaxation. This correction comes closer to the effective exponent $\tilde{x}=0.27$, but improves the description of the effective power law only little, as can be seen in the straight full line with label x'. When including the curvature $b_2=0.0132$ in the approximation, cf. Eq. (16b), we find the dashed curve b_2, which describes the relaxation over three decades in time around the A_3 plateau. But again it covers only the onset of the effective power law. In that sense the effective power law is the analog of the effective logarithmic decay discussed in connection with Fig. 9 of Ref. [12], where a crossover from A_3 to A_2 dynamics could explain the observed decay.

For $D_0^s/D^s\geqslant 10^7$ we observe that the curves in Fig. 8 can be condensed onto a master curve after the gel plateau. This holds for the solutions as well as for the asymptotic approximations since the distance to the A_3 singularity is no longer changed significantly. The decay around the A_3 plateau is part of the α process for the gel transition. This α process contains also the relaxation around the third plateau in Fig. 8 that represents the glass transition at the crossing point.

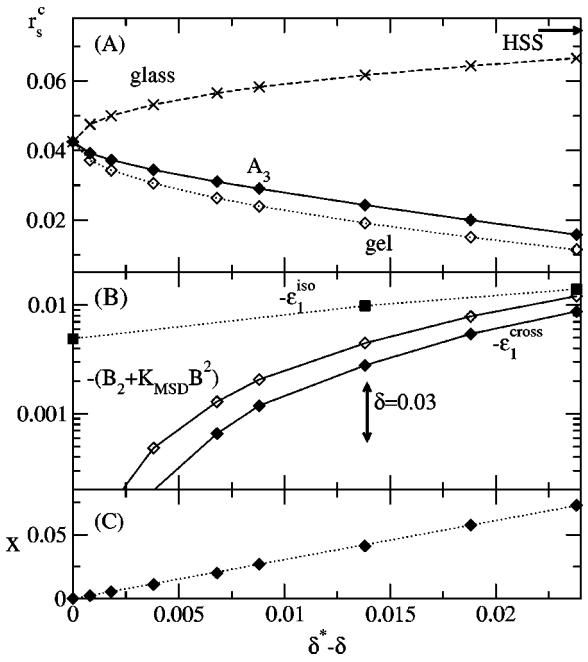

FIG. 9. Variation with the well width. Panel (a) shows the localization length r_s^c at the crossing point for the glass ($\times$) and the gel state ($\diamond$) as a function of $\delta^*-\delta$ together with the value at the A_3 singularity ($\blacklozenge$), $\delta^*=0.043\,81$. The value of r_s^c in the HSS is indicated by the arrow. Panel (b) displays the separation parameter $-\varepsilon_1$ ($\diamond$) and the quadratic corrections to the logarithmic relaxation at the crossing point. For $\delta=\delta^*$,0.03,0.02, the minimal $|\varepsilon_1|$ is displayed ($\blacksquare$) which can be reached on the isodiffusivity line $D_0^s/D^s=10^{10}$. Panel (c) displays the exponents x ($\blacklozenge$), cf. Eq. (15b), and the fit $x=3.05$ $(\delta^*-\delta)$ as dotted line.

Since the distance to this point is relatively large, the asymptotic laws are modified by rather large corrections as indicated by the plateau correction for the curve labeled $D_0^s/D^s=10^{10}$. Despite the larger distance of the connected glass-transition singularity, the last relaxation still slows down the dynamics by one decade before the final crossover to the long-time diffusion.

To demonstrate how the crossing scenario in Fig. 8 changes when δ is varied, Fig. 9 exhibits the parameters relevant for the description of the relaxation. The three plateaus in Fig. 8 are defined by the localization lengths r_s^c. Figure 9(a) shows the variation of the localization lengths. At the A_4 singularity, $\delta=\delta^*$, all three plateaus join in a single localization length. For $\delta<\delta^*$, the localization of a glass state at the crossing is larger than the localization of the gel state. This difference is becoming more pronounced as δ decreases. For the gel the localization follows δ and for the glass the localization approaches the value for the HSS. In between there is the plateau for the A_3 singularity, which closely follows the localization for the gel. This limits the regime for the von Schweidler relaxation after the gel plateau, as observed in connection with Fig. 8, if the A_3 singularity is close. Sufficiently far from higher-order singularities, the amplitude in δr^2 delimited by the localization lengths of gel and glass transition exhibits the dynamics defined by a crossover of two different A_2 singularities. If the

A_3 singularity is close by, as discussed in Fig. 8, logarithmic laws influence the relaxation.

The influence of the A_3 singularity is quantified by the separation parameter at the crossing, $\varepsilon_1^{\rm cross}$, shown for the various crossing points in Fig. 9(b). For smaller δ, the separation increases and limits the A_3 dynamics visible in the relaxation at the crossing. The quadratic correction as dominant deviation from the logarithmic decay laws is governed by the variation of $\varepsilon_1^{\rm cross}$ while the variation in $K_{\rm MSD}$ is only small as noted earlier [32]. If in an experiment one is limited to a dynamical window given by a diffusivity of, say, $D_0^s/D^s=10^{10}$, this implies further restrictions to the detection of the higher-order singularities. The minimal separation on the isodiffusivity curve $D_0^s/D^s=10^{10}$ is shown as $\varepsilon_q^{\rm iso}$ in Fig. 9(b). The exponent x, cf. Eq. (15b), assumed at the crossing point can be used as an estimate for the separation from the A_3 singularity. Since the distance between crossing point and end point varies quadratically in $\delta^*-\delta$, cf. inset of Fig. 3, the exponent x at the crossing is linear in $\delta^*-\delta$, cf. Eq. (13). This is shown in Fig. 9(c) where the exponents can be fitted by a linear function. When restricted to the isodiffusivity curve $D_0^s/D^s=10^{10}$, the exponents are larger, accordingly. For $\delta=0.02$ we find $x=0.169$ and for $\delta=0.03$ the minimal exponent is $x=0.095$.

VI. RESULT FOR THE CORRELATION FUNCTION

The preceding section showed that the dynamical laws at a crossing of liquid-glass transition lines can be quite intriguing since upon variation of control parameters the separation to three different singularities is changed. For the discussion of the density correlators $\phi_q(t)$, there enters the wave number as a further parameter. Allowing also for a variation in q combines the subtle q variation for the logarithmic decay, cf. Ref. [32], with the q dependence of the decay at A_2 singularities. We shall select only a special case which was considered in Ref. [21] and found in an experiment [13,17] and also in MD simulation [15].

Figure 10 shows how the dynamics for the states specified in the inset is described by the asymptotic laws for different singularities. The interesting feature is the straight line piece describing the decay for $0.8\gtrsim\phi_q(t)\gtrsim0.6$ for states 1 and 2. This reflects the logarithmic decay caused by the A_3 singularity. The appropriate plateau value connected with the A_3 singularity is $f_q^\circ=0.899$, and close to the plateau for the gel transition $f_{\rm gel}^c$. That the plateaus for gel transitions and for the A_3 singularity are close for any wave vector is also reflected in the localization lengths in Fig. 9(a). Therefore the logarithmic laws for the A_3 singularity have an asymmetric range of applicability. The range is rather small for shorter times since the gel transition interferes, and considerably larger for longer times as the critical decay due to the glass transition has a more distant plateau.

The evolution of the dynamics when moving from state 1 to state 2 is the analog of the dynamics seen in the MSD in Fig. 5(b). Only a minor part of the slowing down takes place at the gel plateau, the major part from $t\approx8$ to $t\approx10^4$ is described by the logarithmic laws around f_q°. For the solu-

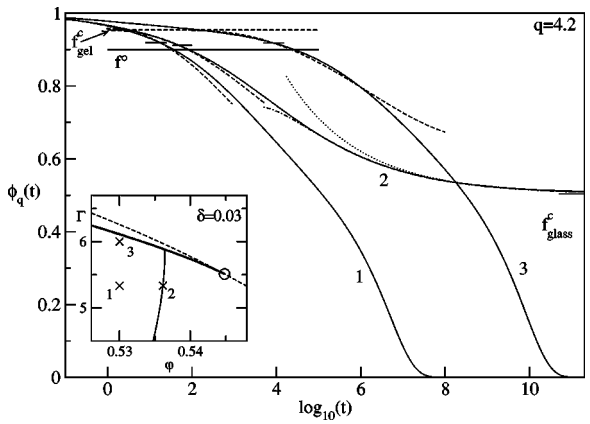

FIG. 10. Logarithmic decay of the density correlation function for $q=4.2$ near the crossing point for $\delta=0.03$. The inset shows part of the glass-transition diagram for $\delta=0.03$ including the line $\varepsilon_1=0$ (dashed). The full curves in the main panel display the solutions for states $n=1,2,3$: $(\Gamma,\varphi)=(0.53,5.33)$, $(5.33,0.5361)$, and $(0.53,6)$ which are marked in the inset. Three relevant plateaus are indicated by horizontal lines for the gel transition (dashed) at $(0.530,6.1)$ labeled $f_{\rm gel}^c$, for the A_3 singularity (full line) labeled f°, and for the glass transition at $(0.536,5.33)$ (short full line) labeled $f_{\rm glass}^c$. The plateau values are $f_{\rm gel}^c=0.954$, $f^\circ=0.899$, and $f_{\rm glass}^c=0.503$. Short lines show the corrected A_3 plateau values $f^\circ+\delta\hat{f}$ for the three states specified. Broken curves show the next-to-leading approximation for the logarithmic decay, dotted and dash-dotted curves the leading and next-to-leading approximation for the critical decay (8) in curve 2 at $f_{\rm glass}^c$.

tions 1 and 2, the approximation by the next-to-leading order is valid from $t\approx10$ to $t\approx10^3$ and 10^4, respectively. At the A_2 singularity for the glass transition, the critical law (8) is observed. The exponent parameter $\lambda=0.847$ implies an exponent $a=0.250$. The leading t^{-a} law (dotted) describes curve 2 successfully for $t\gtrsim10^6$ and adding the correction (dash-dotted) improves that range by almost two decades. Curve 2 demonstrates how different asymptotic expansions complement one another: The logarithmic laws describe the decay from above f_q° down to $\phi_q(t)\gtrsim0.7$ and Eq. (8) approximates successfully the region from $\phi_q(t)\lesssim0.7$ to the critical plateau $f_{\rm glass}^c$. That the slope of the decay becomes smaller below f_q° is a clear indication of a closer approach to a higher order singularity, as prefactor B in Eq. (13) vanishes with the square root of the distance from the A_3 singularity.

When taking another path from 1 to state 3, the distance to the A_3 singularity remains largely unaltered and we find the counterpart of Fig. 8 for the MSD. The dynamics is ruled by an approach to the gel transition and the complete decay below $f_{\rm gel}^c$ is part of the α process. This α process for the gel transition scales by a shift along the respective plateau $f_{\rm gel}^c$ with only minor deviations due to changing separations to the glass-transition line and the A_3 singularity. No clear two-step process is observed for curve 3 for two reasons. First, the A_2 dynamics below $f_{\rm gel}^c$ is limited by the logarithmic laws for the A_3 singularity. Second, the complete decay seen in curve 3 requires more than ten decades, but only for $t\lesssim10^2$ the decay takes place above the plateau $f_{\rm gel}^c$. Hence, the de-

cay onto the plateau is too close to the transient dynamics to exhibit a clear critical decay. Moreover, the exponent parameter in the vicinity of the A_3 singularity is already rather high, $\lambda = 0.89$, so the critical law t^{-a} is stretched considerably. As in the MSD shown in Fig. 8 for the last curve, moving closer to the gel transition, the two-step process typical for an A_2 singularity reemerges.

VII. CONCLUSIONS

The relaxation scenarios for line crossings near higher-order glass-transition singularities were presented in this work. Three different singularities influence the dynamics in that region of the glass-transition diagram, and asymptotic expansions around each of these are necessary to successfully describe the complete relaxation patterns. Each singularity is associated with a characteristic plateau value as shown for the localization lengths for the MSD in Fig. 9(a) and for the Debye-Waller factors f_q^c for $\phi_q(t)$ in Fig. 10. The position of the different plateau values arranges the successive steps for the relaxation in time.

The plateau of the gel transition is encountered first. It is approached by the relaxation with the critical law of the A_2 singularity, cf. Fig. 5(c). The dynamics after crossing the gel plateau is described by the von Schweidler law related to the A_2 singularity for the gel transition, cf. Fig. 8, before the logarithmic laws at the A_3 singularity become valid. The latter have been studied extensively and imply a subdiffusive power law with exponent x, cf. Eq. (15b) for the MSD at specific points in control-parameter space where b_2 in Eq. (16b) vanishes [32]. However, for a region near the crossing where $b_2 > 0$, an effective power law with exponent $\tilde{x}$ can be identified in Fig. 5(c). The onset of this behavior is described by the asymptotic dynamics around the A_3 singularity while the extension to later times originates from a crossover to the critical dynamics at the plateau of the glass transition, cf. Fig. 8. Both the asymptotic power law [16] and the crossover scenario [15] have been found for the MSD in recent computer simulation studies.

A similar crossover which yields the $t^{\tilde{x}}$ relaxation in the MSD is responsible for an effective logarithmic decay in the correlation functions for wave vectors that are accessible in typical light-scattering experiments. Again, the dynamics between the plateau for the A_3 singularity and the plateau for the glass transition assumes a variation linear in $\ln t$, cf. Fig. 10. Most of this behavior is fitted satisfactorily by two different asymptotic laws and is therefore clearly differentiated from the asymptotic logarithmic decay at higher-order singularities which is expected only for large values of the wave vector [32]. Nevertheless, also the effective logarithmic decay can serve as a clear signature of a line crossing and hence for the existence of higher-order singularities. The decay analyzed in Fig. 10 has been identified as a typical scenario in systems with short-ranged attraction in experiment [13], theory [21], and computer simulation [15].

The last relaxation step of the complete decay in the vicinity of the line crossing occurs at the plateau for the glass transition and is similar to the scenario known from the HSS as seen in Fig. 5(a). Only after having crossed this last plateau, the dynamics enters the long-time diffusion limit. Each of the relaxation steps discussed above can be more or less pronounced depending on the separation from the related singularity in control-parameter space. It can be inferred from Figs. 6, 7, and 9 that in a certain region around the higher-order singularities, the presence of the latter singularities introduces large corrections to the asymptotic laws at gel- and glass-transition points. Outside this region, however, the use of the conventional A_2 scenario is justified and the asymptotic approximation varies only little there. Hence, the dynamics near any state on the entire surface of liquid-glass and liquid-gel transitions can be characterized by the parameters of the asymptotic approximations.

The variation of the final long-time diffusion can be used to map the theoretical glass-transition diagram to the experimental control-parameter space and thus locate higher-order glass-transition singularities at least approximately. The mapping proposed in this work could be used to estimate the location of an A_3 singularity in Ref. [15] by extrapolation, cf. Fig. 4, and facilitated the identification of an A_4 singularity in a recent computer simulation study [16]. Within the Percus-Yevick approximation for S_q, the A_3 singularities are behaving similar to the critical points of the fcc-fcc binodal [45]. Upon changing the well width δ, MCT end points and critical points vary only little in the attraction strength Γ as seen in Fig. 3. When using the structure factor in mean-spherical approximation, this behavior is different. But this difference is eliminated after identifying the glass-transition diagrams for both closure relations at the crossing points. For $\delta = 0.03$, the densities of end point and critical point are in accord reasonably, while the higher value for Γ fixes the A_3 singularity in the metastable region with respect to the isostructural phase transition.

Note added in proof. For an additional colloidal system, the measured correlation functions could be interpreted as a crossing scenario close to an end point singularity in a very recent work [50].

ACKNOWLEDGMENTS

I thank W. Götze for a valuable discussion. This work was supported by the Deutsche Forschungsgemeinschaft Grant No. Go154/13-1.

APPENDIX: CONSISTENCY OF THE NUMERICAL SOLUTION

Glass-glass-transition points and higher-order singularities were calculated for Figs. 1–3, and 9. The expeditious and accurate identification of these singularities is also crucial for the evaluation of the asymptotic approximations. Therefore, some notes concerning the numerical solution of Eq. (2) shall be discussed in this appendix. For the determination of liquid-glass-transition points a robust method of nested intervals can be applied anticipating the jump from

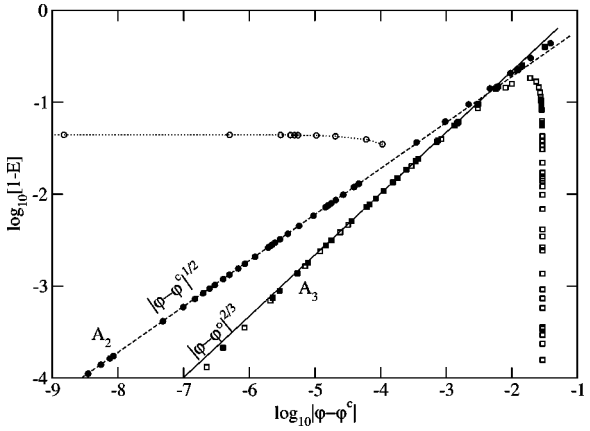

FIG. 11. Eigenvalues E upon approaching a glass-glass transition for $\delta=0.02$, $\Gamma=7.75$, and $\varphi^c=0.540\,965\,015$. The deviation from unity, $1-E$, is shown for $\varphi<\varphi^c$ (open circles) and for $\varphi>\varphi^c$ (filled circles) together with the square root $\sqrt{|\varphi-\varphi^c|}$ (dashed). The corresponding eigenvalues for the A_3 singularity at $\delta=0.02$, $\Gamma^\circ=6.646$, and $\varphi^\circ=0.568\,032\,1$ are denoted by open squares for $\varphi<\varphi^\circ$ and by the filled squares for $\varphi>\varphi^\circ$. The full line shows the power law $|\varphi-\varphi^\circ|^{2/3}$.

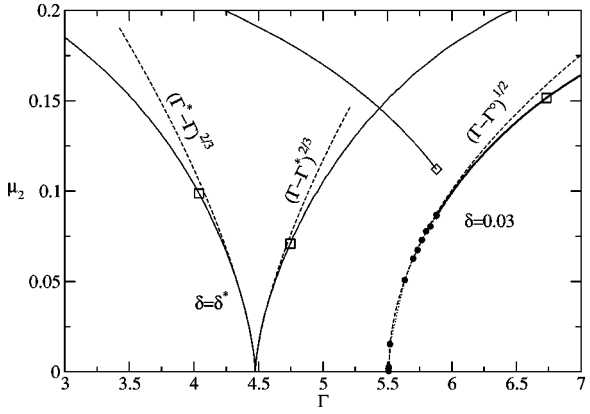

FIG. 12. Parameter $\mu_2=1-\lambda$ in the SWS for $\delta=\delta^*$ and 0.03. Values for liquid-glass transitions are shown as full lines, for glass-glass transitions as filled circles. The dashed lines show the laws $\mu_2\propto(\Gamma-\Gamma^*)^{2/3}$ for the A_4 singularity and $\mu_2\propto(\Gamma-\Gamma^\circ)^{2/3}$ for the A_3 singularity. The squares indicate a deviation between result and approximation of 5%.

zero to a finite value in the glass-form factors f_q at the respective A_2 singularity. This procedure works also at an A_4 singularity which is also a liquid-glass-transition point. For a glass-glass-transition point the discontinuity in the glass-form factors takes place between finite values and the jump in the f_q becomes smaller when approaching the A_3 singularity and observing a discontinuity in the glass-form factors becomes increasingly difficult. Therefore a different criterion shall be used. To this end, coefficients from the expansion of the right-hand side of Eq. (2) are required, cf. [12],

$$A^{(n)c}_{qk_1\cdots k_n}=\frac{1}{n!}(1-f^c_q)\{\partial^n\mathcal{F}_q[\mathbf{V}^c,f^c_k]/\partial f^c_{k_1}\cdots\partial f^c_{k_n}\}\times(1-f^c_{k_1})\cdots(1-f^c_{k_n}). \tag{A1}$$

At a glass-transition singularity, Eq. (2) is no longer invertible which is signaled by the maximum eigenvalue E of the so-called stability matrix $A^{(1)c}_{qk}$ approaching unity from below [3]. The evolution of E in the vicinity of an A_2 singularity is given by a square root in some control parameter v, $1-E\propto\sqrt{v-v^c}$, for the strong-coupling side $v>v^c$. Monitoring the eigenvalues can be done with high precision and allows for an extrapolation in control parameters which can reduce the numerical effort considerably. At an A_3 singularity, the eigenvalue is approaching unity from either side on generic paths in control-parameter space through the singularity. The variation is given by $1-E\propto(v-v^\circ)^{2/3}$ which follows from generic properties of the singularity [49].

It is clearly seen in Fig. 11 that at a glass-glass transition only the eigenvalues for the strong coupling side, $\varphi>\varphi^c$, go to unity and follow the square-root law. At a liquid-glass transition the eigenvalues for $\varphi<\varphi^c$ would be zero, however, in the glass due to continuity they are finite, smaller than unity and jump to a critical value only at the glass-glass-transition points. For the A_3 singularity this discontinuity vanishes and the eigenvalues show the variation with the power 2/3 on both sides of φ°. The deviation from that law for larger distances with $\varphi<\varphi^\circ$ is due to the increase of the eigenvalues at the liquid-glass transition at $\varphi=0.540\,693$. Deviations close to the A_3 singularity on the other hand indicate the precision of five digits in the control parameter φ for the determination of $\mathbf{V}^\circ$. The deviation of E^c from unity is a measure for the accuracy of the critical points. In this work a value of $1-E^c\leqslant10^{-3}$ was assured for all the transition points shown in this work.

Despite being useful as an extrapolation scheme, the generic laws close to the singularities can also serve as consistency check for the numerical results. This was already shown in the inset of Fig. 3 for the distance of the crossing point from the A_3 singularity. There, the control parameters close to the A_4 singularity were related in a quadratic polynomial. As another quantity we utilize the exponent parameter λ which approaches unity at higher-order singularities. $\mu_2=1-\lambda$ is also given by coefficients from Eq. (A1), $\mu_2=1-a^*_qA^{(2)c}_{qk_1k_2}a_{k_1}a_{k_2}$, where summation over repeated indices is assumed and a^*_q and a_q denote the left and right eigenvectors of the stability matrix $A^{(1)c}_{qk}$, respectively.

Figure 12 shows that close to higher-order glass-transition singularities the exponent parameters $\lambda=1-\mu_2$ calculated numerically obey the asymptotic approximation by the respective power laws with reasonable accuracy. For the A_3 singularity the description works down to $\lambda=0.85$ and includes both glass-glass transitions and liquid-gel transitions. The A_4 singularity is described by the asymptotic law for $\lambda\geqslant0.93$ on the line of gel transitions and for $\lambda\geqslant0.9$ on the line of glass transitions. The exponent parameters for different potentials fall on top of each other close to their A_4 singularities [24]. That the asymptotic approximation is applicable for a similar range in control parameters underlines the universality of the A_4 singularity.

[1] U. Bengtzelius, W. Götze, and A. Sjölander, J. Phys. C **17**, 5915 (1984).
[2] W. Götze, in *Liquids, Freezing and Glass Transition*, Proceedings of the Les Houches Summer Schools of Theoretical Physics, edited by J. P. Hansen, D. Levesque, and J. Zinn-Justin (North-Holland, Amsterdam, 1991), Vol. Session LI, pp. 287–503.
[3] W. Götze and L. Sjögren, J. Math. Anal. Appl. **195**, 230 (1995).
[4] V. I. Arnol'd, *Catastrophe Theory*, 3rd ed. (Springer, Berlin, 1992).
[5] T. Franosch, M. Fuchs, W. Götze, M.R. Mayr, and A.P. Singh, Phys. Rev. E **55**, 7153 (1997).
[6] M. Fuchs, W. Götze, and M.R. Mayr, Phys. Rev. E **58**, 3384 (1998).
[7] P.N. Pusey and W. van Megen, Nature (London) **320**, 340 (1986).
[8] W. van Megen and S.M. Underwood, Phys. Rev. Lett. **70**, 2766 (1993).
[9] W. van Megen and S.M. Underwood, Phys. Rev. E **49**, 4206 (1994).
[10] W. van Megen, Transp. Theory Stat. Phys. **24**, 1017 (1995).
[11] W. Götze and R. Haussmann, Z. Phys. B: Condens. Matter **72**, 403 (1988).
[12] W. Götze and M. Sperl, Phys. Rev. E **66**, 011405 (2002).
[13] F. Mallamace, P. Gambadauro, N. Micali, P. Tartaglia, C. Liao, and S.-H. Chen, Phys. Rev. Lett. **84**, 5431 (2000).
[14] A.M. Puertas, M. Fuchs, and M.E. Cates, Phys. Rev. Lett. **88**, 098301 (2002).
[15] E. Zaccarelli, G. Foffi, K.A. Dawson, S.V. Buldyrev, F. Sciortino, and P. Tartaglia, Phys. Rev. E **66**, 041402 (2002).
[16] F. Sciortino, P. Tartaglia, and E. Zaccarelli, e-print cond-mat/0304192.
[17] W.-R. Chen, S.-H. Chen, and F. Mallamace, Phys. Rev. E **66**, 021403 (2002).
[18] S.-H. Chen, W.-R. Chen, and F. Mallamace, Science **300**, 619 (2003).
[19] L. Fabbian, W. Götze, F. Sciortino, P. Tartaglia, and F. Thiery, Phys. Rev. E **59**, R1347 (1999); **60**, 2430(E) (1999).
[20] J. Bergenholtz and M. Fuchs, Phys. Rev. E **59**, 5706 (1999).
[21] K. Dawson, G. Foffi, M. Fuchs, W. Götze, F. Sciortino, M. Sperl, P. Tartaglia, T. Voigtmann, and E. Zaccarelli, Phys. Rev. E **63**, 011401 (2001).
[22] K.A. Dawson, G. Foffi, G.D. McCullagh, F. Sciortino, P. Tartaglia, and E. Zaccarelli, J. Phys.: Condens. Matter **14**, 2223 (2002).
[23] G. Foffi, G.D. McCullagh, A. Lawlor, E. Zaccarelli, K.A. Dawson, F. Sciortino, P. Tartaglia, D. Pini, and G. Stell, Phys. Rev. E **65**, 031407 (2002).
[24] W. Götze and M. Sperl, J. Phys.: Condens. Matter **15**, S869 (2003).
[25] W. B. Russel, D. A. Saville, and W. R. Schowalter, *Colloidal Dispersions* (Cambridge University Press, New York, 1989).
[26] W.C.K. Poon, J. Phys.: Condens. Matter **14**, R859 (2002).
[27] T. Eckert and E. Bartsch, Phys. Rev. Lett. **89**, 125701 (2002).
[28] K.N. Pham, A.M. Puertas, J. Bergenholtz, S.U. Egelhaaf, A. Moussaïd, P.N. Pusey, A.B. Schofield, M.E. Cates, M. Fuchs, and W.C.K. Poon, Science **296**, 104 (2002).
[29] G. Foffi, K.A. Dawson, S.V. Buldyrev, F. Sciortino, E. Zaccarelli, and P. Tartaglia, Phys. Rev. E **65**, 050802 (2002).
[30] A.M. Puertas, M. Fuchs, and M.E. Cates, Phys. Rev. E **67**, 031406 (2003).
[31] W. Götze, J. Phys.: Condens. Matter **11**, A1 (1999).
[32] M. Sperl, Phys. Rev. E **68**, 031405 (2003).
[33] W.C.K. Poon, K.N. Pham, S.U. Egelhaaf, and P.N. Pusey, J. Phys.: Condens. Matter **16**, S269 (2003).
[34] T. Eckert and E. Bartsch, Faraday Discuss. **123**, 51 (2003).
[35] L. Sjögren, J. Phys.: Condens. Matter **3**, 5023 (1991).
[36] S. Flach, W. Götze, and L. Sjögren, Z. Phys. B: Condens. Matter **87**, 29 (1992).
[37] I.C. Halalay, J. Phys.: Condens. Matter **8**, 6157 (1996).
[38] H. Eliasson, Phys. Rev. E **64**, 011802 (2001).
[39] M. Fuchs, W. Götze, I. Hofacker, and A. Latz, J. Phys.: Condens. Matter **3**, 5047 (1991).
[40] G. Szamel and H. Löwen, Phys. Rev. A **44**, 8215 (1991).
[41] M. Fuchs, Ph.D. thesis, TU München, 1993 (unpublished).
[42] J.-p. Hansen and I. R. McDonald, *Theory of Simple Liquids*, 2nd ed. (Academic Press, London, 1986).
[43] M. Fuchs, I. Hofacker, and A. Latz, Phys. Rev. A **45**, 898 (1992).
[44] W. Götze, J. Stat. Phys. **83**, 1183 (1996).
[45] P. Bolhuis, M. Hagen, and D. Frenkel, Phys. Rev. E **50**, 4880 (1994).
[46] M. Nauroth and W. Kob, Phys. Rev. E **55**, 657 (1997).
[47] J. Bergenholtz, W.C.K. Poon, and M. Fuchs, Langmuir **19**, 4493 (2003).
[48] W. Götze, J. Phys.: Condens. Matter **2**, 8485 (1990).
[49] M. Sperl, Ph.D. thesis, TU München, 2003 (unpublished).
[50] K.N. Pham, S.U. Egelhaaf, P.N. Pusey, and W.C.K. Poon, Phys. Rev. E (to be published), e-print cond-mat/0308250.